Generation of Coherent X-rays in the Water Window Using 5-Femtosecond Laser Pulses

Ch. Spielmann, N. H. Burnett, S. Sartania, R. Koppitsch, M. Schnürer, C. Kan, M. Lenzner, P. Wobrauschek, F. Krausz*

Coherent extreme-ultraviolet radiation extending to wavelengths below the carbon K edge at 4.37 nanometers (nm) has been generated at a repetition rate of 1 kilohertz by focusing 5-femtosecond near-infrared (780 nm) laser pulses into a helium gas jet. The incident light field performs just a few oscillations, which results in the emission of an x-ray supercontinuum rather than discrete harmonics. Owing to the extremely short rise time of the driving pulses, neutral atoms can be exposed to high fields before they are depleted by ionization. As a result, the observed x-ray radiation extends well into the water window and is delivered in a well-collimated beam (divergence less than 1 milliradian). The high repetition rate and spatial coherence result in a brightness of about 5×10^8 photons per square millimeter per square milliradian per second in a 1-percent bandwidth at 4.37 nm, the carbon edge of the water window. The compact laboratory system holds promise as a source for biological holography and nonlinear optics in the x-ray regime.

Motivation for the development of coherent x-ray sources comes from many areas of science and technology. One of the greatest challenges is the three-dimensional observation of microscopic biological structures (for example, cells and macromolecules) in the living state by means of x-ray holography (*1*). Sources intended for this application must exhibit a high degree of spatial coherence and a reasonable temporal coherence and must provide a good contrast of the substance to be imaged with respect to its surrounding. The latter requirement can be met in the wavelength range between the K absorption edges of carbon (4.37 nm) and oxygen (2.33 nm), which is referred to as the "water window," where carbon-containing biological objects absorb radiation efficiently but water is comparatively transparent. This spectral window for high-contrast biological spectroscopy has set, in terms of wavelength, one of the most important objectives for the research and development of sources of coherent soft x-rays.

So far, coherent radiation in the water window could be demonstrated only in large-scale facilities, through the use of either magnetic undulators in electron storage rings (*2*) or a multikilojoule laser (*3*) to produce a plasma-column x-ray amplifier (*4*). Here we describe a high–repetition-rate laboratory source of coherent water-window radiation. The x-rays emerge from an ensemble of helium atoms coherently driven by quasi–single-cycle light pulses produced by a table-top laser. The underlying physical mechanism is closely related to that responsible for the emergence of high-order harmonics from a gas jet exposed to intense laser radiation. It is hoped that this compact source will make the power of water-window radiation available to many more biochemists and biophysicists than was previously possible. In addition, it offers the possibility of extending nonlinear optics into the x-ray regime and studying atomic processes with attosecond time resolution.

Atoms ionized by strong laser fields can emit coherent harmonic radiation at photon energies much higher than the atomic binding energy (*5*). For femtosecond pulses (duration $\tau_p \approx 100$ fs), harmonic orders exceeding 100 with photon energies up to 150 eV have been observed (*6*). This phenomenon has subsequently been extensively studied both experimentally and theoretically (*7–9*). The semiclassical model of a single active electron put forward independently by Corkum (*8*) and Kulander *et al.* (*10*) explains the emission of high-harmonic radiation in terms of three discrete steps. First, the electron tunnels through the barrier formed by the atomic Coulomb potential and the laser field. The quasi-free electron subsequently acquires kinetic energy from the laser field, and some half of an optical cycle later, it is returned (by the linearly polarized field) to its parent ion. With some (small) probability, the electron recombines to the ground state, emitting a photon with the energy of the ionization potential of the atom plus the kinetic energy gained in the laser field. The process is repeated periodically in the field of a driving pulse consisting of many cycles and gives rise to the emission of harmonics of the incident radiation. The photon energy of the highest harmonic has been predicted as (*7, 8*)

$$(\hbar\omega)_{max} \approx I_p + 3.17U_p \qquad (2)$$

here, I_p is the atomic ionization potential and

$$U_p = e^2E^2/4m\omega_0^2 \qquad (3)$$

is the mean kinetic (or ponderomotive) energy of the electron quivering in the laser field (E is the amplitude of the electric field, ω_0 is the laser frequency, and e and m are the charge and rest mass of the electron, respectively). The magnitude of the second term in Eq. 1 is roughly dictated by the maximum laser intensity that neutral atoms can be exposed to before they are depleted by ionization (*11*). This critical intensity is higher for driver pulses of shorter duration (*12*); hence, they hold the promise of producing harmonics at higher photon energies. In fact, the shortest-wavelength harmonics have been previously generated with the shortest driver pulses available ($\tau_p = 25$ fs) (*13*), in helium down to wavelengths as short as 5.2 nm at a 10-Hz repetition rate (*14*), and longer-wavelength harmonics were also demonstrated at repetition rates of a few hundred hertz (*15*).

Dramatic advances in ultrashort-pulse laser technology have recently led to the generation of laser pulses with a duration as short as 5 fs and a peak power of 0.1 TW in a diffraction-limited beam at a repetition rate of 1 kHz (*16*). This performance has been achieved with a compact, table-top, solid-state laser system using a Ti:sapphire oscillator, an amplifier, and a hollow-fiber–chirped-mirror compressor (*16, 17*). The electric field performs just a few oscillations in these pulses (Fig. 1), which are carried at wavelength $\lambda \approx 780$ nm and have an oscillation period of 2.6 fs. Here we show experimentally that being focused in a helium gas jet, these "light transients" are capable of generating spatially coherent extreme ultraviolet (xuv) supercontinuum extending below the carbon K edge.

The helium gas target is formed by a thin nickel tube having a wall thickness of 0.05 mm and an inner diameter of 0.6 mm, which is squeezed to about 30 μm (Fig. 2) (*18*). The laser beam is focused with a silver-coated spherical mirror (focal length, 20 cm) through an 0.3-mm-thick fused silica window into a vacuum chamber containing the target at focus. The

Ch. Spielmann, S. Sartania, R. Koppitsch, M. Schnürer, M. Lenzner, F. Krausz, Abteilung Quantenelektronik und Lasertechnik, Technische Universität Wien, Gusshausstrasse 27, A-1040 Wien, Austria.
N. H. Burnett and C. Kan, Department of Electrical Engineering, University of Alberta, Edmonton T6G 2G7, Canada.
P. Wobrauschek, Atominstitut der Österreichischen Universitäten, Schüttelstrasse 115, A-1020 Wien, Austria.

*To whom correspondence should be addressed. E-mail: krausz@ps1.iaee.tuwien.ac.at

holes in the tube wall were bored by the laser beam itself, minimizing the gas load to the surrounding vacuum. Relay imaging revealed a somewhat elliptic, nearly Gaussian intensity profile on target with $1/e^2$ diameters of 50 and 70 μm. The ellipticity is caused by the off-axis spherical focusing mirror. In the experiments described below, the pulse energy was ~0.3 mJ on target, implying a peak intensity of $\approx 4 \times 10^{15}$ W cm^{-2} on the beam axis (*19*). The tube was continuously backed with pressures of 3 to 5 bar, which resulted in a pressure of ≈0.5 bar in the interaction region (*20*). The target chamber was evacuated to ≈1 mbar. The x-ray radiation produced collinearly with the laser beam was passed through a 1-mm aperture (placed ≈35 cm behind the target) into a 1-m grazing-incidence monochromator (248/310G, McPherson, Acton, MA) evacuated to $<10^{-4}$ mbar. The monochromator is equipped with a platinum-coated grating with 300 lines per millimeter and an uncoated channeltron (4715G, Galileo, Sturbridge, MA). The detector signal was collected by a high–dynamic-range lock-in amplifier triggered by the laser pulse train.

Figure 3 depicts the xuv spectrum emitted in the wavelength range from 110 to 10 nm. The monochromator was scanned with the entrance and exit slit widths kept constant, implying a wavelength-dependent bandwidth. The entrance slit located ≈50 cm downstream of the target blocks an increasing fraction of the incident xuv beam for increasing wavelengths (because of wavelength-dependent beam size). Correction for these effects is expected to increase the spectral intensity at long wavelengths by more than an order of magnitude relative to the short-wavelength components. At photon energies below ≈25 eV (corresponding to a wavelength of ≈50 nm), well-resolved odd harmonics are observed. Above 25 eV, the harmonics merge, forming a supercontinuum, as predicted by recent theoretical work (*21*, *22*). Near the transition from harmonics to continuum, what appears to be even harmonics are also present (the most prominent peaking at a wavelength corresponding to the 12th harmonic of the driving radiation), the origin of which needs further investigation. The high-energy cutoff of the continuum cannot be assessed from this measurement, in which the full broadband xuv output from the target is directed into the monochromator, because of the rapidly increasing amount of stray xuv rays leaking through as the zeroth order is approached with the leakage becoming dominant at $\lambda < 8$ nm in the spectrum shown in Fig. 3.

To suppress the zeroth-order throughput, we placed a 100-nm silver foil (fixed on a nickel mesh) in front of the entrance slit. This filter has a nearly constant transmittance (≈50%) between 3 to 10 nm and blocks radiation with wavelengths greater than 10 nm. The short-wavelength tail of the xuv continuum transmitted through the silver filter, obtained by averaging three scans, is shown along with the standard deviation at discrete wavelengths in Fig. 4. Between wavelengths of 4.4 and 4.2 nm, the spectral intensity in a 0.05-nm bandwidth yields a signal that exceeds the noise floor (signal observed with either the laser or the gas flow blocked) of our detection system by a factor of ≈500. In order to check the calibration of our monochromator and provide additional evidence for the emergence of water-window radiation from the He target, the silver filter was replaced by a pair of 900-nm-thick Mylar foils ($C_{10}H_8O_4$). This filter provides an absorption contrast of $>10^3$ at 4.37 nm, the K edge of carbon. The measured soft x-ray spectrum (Fig. 5) exhibits a sharp edge at 4.37 nm, providing a conclusive evidence for water-window radiation. The signal contrast at the carbon K edge was >300, limited by the noise floor of the detection system. From these measurements, the number of photons per pulse emitted within a 1% bandwidth at the carbon K edge is estimated as 100 (*23*).

In the 3- to 4-nm range, we also observe a signal that exceeds the detection limit by more than an order of magnitude (Fig. 4). However, at wavelengths of around 3 nm or shorter, the exit slit is close to the central image (zeroth order) of the monochromator, and a reliable assessment of some possible contribution of zeroth-order stray light to the observed sig-

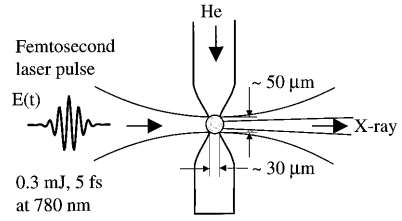

Fig. 2. Schematic of the target geometry for xuv continuum generation.

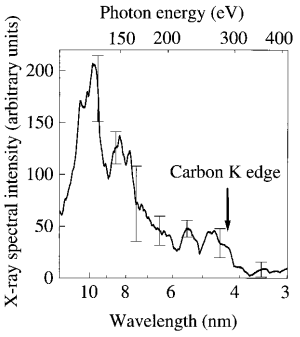

Fig. 4. Short-wavelength end of the xuv continuum as transmitted by a 100-nm-thick silver foil. The depicted spectrum is the average of three scans, and the bars give the respective standard deviation. The spectral components at $\lambda > 10$ nm are damped by the silver foil.

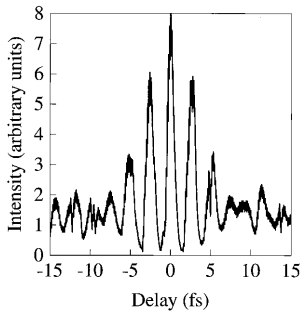

Fig. 1. Second-order interferometric autocorrelation trace of the 5-fs laser pulses used in the experiment. The fringe spacing is ≈2.6 fs, corresponding to the light oscillation cycle at wavelength λ = 780 nm.

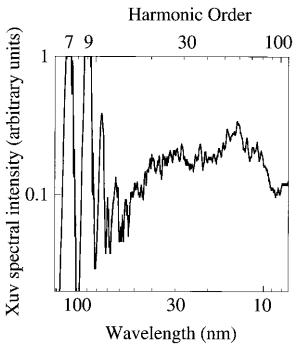

Fig. 3. Broadband (spatially) coherent xuv output from He on a logarithmic scale. The spectrum was recorded with an entrance and exit slit width of 100 μm, corresponding to a bandwidth of ~0.02 nm at λ = 10 nm and ~0.06 nm at λ = 100 nm.

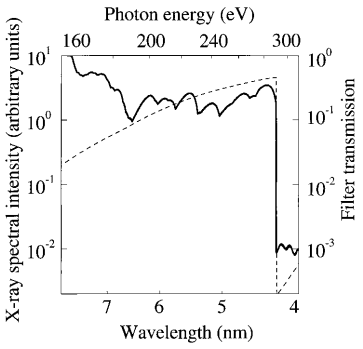

Fig. 5. Short-wavelength end of the xuv spectrum as transmitted by a 1.8-μm-thick Mylar foil (solid line) and the transmittance of the foil (dashed line).

nal is difficult. This short-wavelength edge of the spectrum has therefore also been studied with an energy-dispersive detection system (Z-MAX, NORAN Instruments, Middleton, WI) consisting of a cooled lithium-drifted silicon-crystal detector and a multichannel pulse height analyzer. After the number of counts per laser shot had been reduced to far below unity ($\approx$0.01) and the low-energy photons (E_{ph} < 100 eV) had been suppressed by suitable filtering, this system yielded reliable information on the photon energy distribution of the emitted x-ray radiation for photon energies higher than 0.2 keV (λ < 6 nm) (*24*). Under the experimental conditions described above, the coherent x-ray spectrum extended to photon energies exceeding 0.5 keV, which correspond to wavelengths shorter than 2.5 nm. Correction for filter transmittances resulted in x-ray intensities at around 2.5 nm, some three orders of magnitude lower than observed at 4.4 nm, which suggests that the spectrum shown in Fig. 4 is likely to contain a considerable stray-light component at around 3 nm.

The observed shape of the high-energy end of the emitted x-ray spectrum strongly deviates from that of the single-atom response as predicted by recent modeling (*22*). In fact, the radiation spectrum of a He atom driven by a 5-fs pulse exhibits a broad plateau of nearly constant intensity. The plateau extends to the photon energies given approximately by Eqs. 1 and 2, with E being the peak electric field of the laser pulse unless neutral atoms are substantially depleted by ionization before exposure to the pulse peak. Assuming the ADK model for tunnel ionization to be valid (*25*), the depletion is completed at a peak intensity of $\approx 4 \times 10^{15}$ W cm^{-2} with a 5-fs pulse. Drawing on the ADK model, our simulations yielded, in reasonable accordance with Eq. 1, a cutoff in the single-atom radiation spectrum above 0.5 keV (below 2.5 nm) for a peak intensity of 3 $\times$ 10^{15} W cm^{-2}. The striking discrepancy between the predicted plateau up to these photon energies and the experimentally observed rapid intensity roll-off for increasing photon energies points to the dramatically increasing role of dephasing between the fundamental- and high-frequency waves during propagation across the target. This dephasing is caused by an accumulating phase error due to plasma dispersion and wave front curvature, which rapidly increases for decreasing x-ray wavelengths.

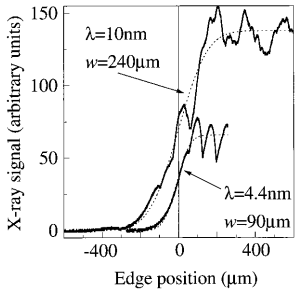

Fig. 6. Transmitted x-ray power as a function of the position of an opaque knife edge scanning transversely (in vertical direction) across the beam profile 29 cm from the He target at two different wavelengths (10 nm and 4.4 nm). The dotted lines depict Gaussian fits to the measured profiles.

Several experiments have been performed to check if incoherent plasma emission from the walls of the target tube or the high-pressure gas target, or both, contribute to the observed signal. First, deliberate misalignment of the laser beam to graze the tube wall in vacuum resulted in no measurable signal. Second, replacing helium with argon while keeping all other experimental parameters unchanged yielded no signal transmitted through the silver foil, although the electron density was significantly higher because of the lower ionization potential. Furthermore, increasing the pulse duration at constant pulse energy caused the short-wavelength edge of the spectrum to retreat to longer wavelengths. These tests, along with the well-collimated nature of the emission, provide conclusive evidence for the coherent harmonic emission process being responsible for the detected radiation.

The usefulness of this source for applications greatly depends on the spatial coherence of the emitted radiation. In order to estimate the degree of spatial coherence and, what is closely related with it, the brightness of the generated short-wavelength radiation, we have investigated the spatial profile of the x-ray radiation by scanning a knife edge transversely across the beam (*26*). The transmitted power measured as a function of the edge position with respect to the propagation axis at a position 29 cm from the He target is shown in Fig. 6 at two different wavelengths (10 and 4.4 nm). If we assume a Gaussian intensity profile $I(r) \propto \exp(-2r^2/w^2)$, the best fits to the measured data yield a $1/e^2$ diameter of $2w$ = 480 and 180 μm at λ = 10 and 4.4 nm, respectively. In the case of perfect spatial coherence, these data would imply a beam diameter of $2w_{0,ideal} \approx 10$ μm at the beam waist, a value that is merely some factor of 3 smaller than the diameter of the interaction region in which these high photon energies can be produced. The good spatial coherence results in a small divergence, which, together with the high repetition rate, gives rise to a high brightness. If we assume that the x-ray beam diameter is $2w_0 \approx 25$ μm at the beam waist (*27*), we estimate the brightness of the presented source at the carbon K edge within a 1% bandwidth as 5×10^8 photons mm^{-2} mrad^{-2} s^{-1}. Because the coherence length for generating water-window radiation is currently likely to be limited by geometric phase matching (*18*), higher pulse energies allowing more gentle focusing are expected to result in improved efficiency. Upgrade of the laser system to pulse energies of a few millijoules and further optimization of the xuv generation process should boost the brightness by at least 2 orders of magnitude, making this compact laboratory source a powerful tool for high-resolution biological microscopy and holography.

Our simulations including propagation (*28*) have revealed that a key parameter for optimizing the x-ray source for maximum brightness at high photon energies is the relative carrier phase ψ of the 5-fs pulses (*29*). The value of ψ appears to affect the x-ray fluence in the cutoff region by an order of magnitude. Because ψ is not controlled and hence cannot be kept constant in our laser pulses currently, this theoretically predicted phase sensitivity of the x-ray spectrum may explain the large fluctuations observed in the x-ray intensity at wavelengths < 10 nm in spite of the relatively small energy fluctuation of the 5-fs pulses (<5%). As a consequence, the carrier phase will have to be controlled (*30*) in the next generation of coherent soft x-ray sources, driven by sub–10-fs pulses.

Finally, we briefly address the temporal evolution of the radiation emitted at wavelengths less than 10 nm and its implications. Our simulations indicate, in accordance with previous work (*21, 22*), that the short-wavelength end of the continuum is emitted within a single burst lasting less than 1 fs. According to these simulations blocking radiation at wavelengths longer than 10 nm (silver filter) and 5 nm (titanium filter), the He ensemble irradiated by the 5-fs pulse emits a single attosecond x-ray pulse with a duration of <0.3 fs and <0.2 fs, respectively. Our analysis underlines the crucial role of propagation and phase matching in this single-pulse selection. For the wavelength range near the carbon K edge, this temporal evolution implies a peak intensity of >10^6 W cm^{-2} on the propagation axis behind the He target. Significantly higher x-ray intensities can be obtained at somewhat longer wavelengths (10 to 20 nm), owing to an increased coherence length related to weaker ionization. The predicted intense x-ray pulses delivered in a nearly diffraction-limited beam along with the sensitive detection

techniques available at kilohertz repetition rates offer the potential for attosecond-resolution atomic spectroscopy and nonlinear optics in the x-ray regime.

REFERENCES AND NOTES

1. J. C. Solem and G. C. Baldwin, *Science* **218**, 229 (1982); M. Howells *et al.*, *ibid.* **238**, 514 (1987); J. E. Trebes *et al.*, *ibid.*, p. 517.
2. D. Attwood, K. Halbach, K.-J. Kim, *ibid.* **228**, 1265 (1985).
3. B. J. Macgowan *et al.*, *Phys. Rev. Lett.* **65**, 420 (1990).
4. Flash x-ray sources such as those demonstrated in (*3*) would be ideal for the avoidance of image blurring due to, for example, object motion during exposure [R. A. London *et al.*, *Appl. Opt.* **28**, 3397 (1989)]; however, the spatial coherence of the sources demonstrated in the water window so far are far from being sufficient for single-shot biological holography.
5. A. McPherson *et al.*, *J. Opt. Soc. Am. B* **4**, 595 (1987); X. F. Li *et al.*, *Phys. Rev. A* **39**, 5751 (1989).
6. A. L'Huillier and Ph. Balcou, *Phys. Rev. Lett.* **70**, 774 (1993); J. J. Macklin *et al.*, *ibid.*, p. 766.
7. J. L. Krause *et al.*, *ibid.* **68**, 3535 (1992).
8. P. B. Corkum, *ibid.* **71**, 1995 (1993).
9. M. Lewenstein *et al.*, *Phys. Rev. A* **49**, 2117 (1994).
10. K. C. Kulander *et al.*, in *Proceedings of the Workshop on Super-Intense Laser Atom Physics (SILAP) III*, P. Piraux, Ed. (Plenum, New York, 1993).
11. K. Miyazaki and H. Takada, *Phys. Rev. A* **52**, 3007 (1995).
12. I. P. Christov *et al.*, *Phys. Rev. Lett.* **77**, 1743 (1996); K. J. Schafer and K. C. Kulander, *ibid.* **78**, 638 (1997).
13. J. Zhou *et al.*, *ibid.* **76**, 752 (1996).
14. Z. Chang *et al.*, in *Applications of High Field and Short Wavelength Sources VII* (*OSA Tech. Digest Ser.*, vol. 7, Optical Society of America, Washington, DC, 1997), p. 187.
15. R. Haight and P. F. Seidler, *Appl. Phys. Lett.* **65**, 517 (1994).
16. S. Sartania *et al.*, *Opt. Lett.* **22**, 1562 (1997).
17. M. Nisoli *et al.*, *ibid.*, p. 522.
18. Given the finite tube wall thickness of 0.05 mm, the actual target thickness is estimated as 100 to 200 μm. The coherence length related to the phase error introduced by the tight focusing of the fundamental (*11*) is on the order of 10 μm for wavelengths shorter than 10 nm. The target thickness has been minimized in an attempt to keep the interaction length as close as possible to this "geometric" coherence length. It is this geometric coherence length limitation that dictates the necessity of the high pressures applied.
19. Note that this peak irradiance is reached only on the propagation axis in an infinitesimally small fraction of the cross section of the Gaussian beam. The majority of the helium atoms in the interaction volume are exposed to somewhat lower irradiances.
20. The pressure in the interaction region has been estimated as follows. The gas flow from the target region into the chamber is calculated from the known pumping speed and the measured background pressure in the target chamber. Gas flow and background pressure then determine uniquely the pressure in the target.
21. I. P. Christov *et al.*, *Phys. Rev. Lett.* **78**, 1251 (1997).
22. C. Kan *et al.*, *ibid.* **79**, 2971 (1997).
23. We used a detector quantum efficiency of 2%, an electron multiplication gain of 5×10^6, and a grating diffraction efficiency of 10% (data provided by the manufacturers) for this estimation.
24. M. Schnürer *et al.*, unpublished results.
25. M. V. Ammosov *et al.*, *Zh. Eksp. Teor. Fiz.* **91**, 2008 (1986) [*Sov. Phys. JETP* **64**, 1191 (1986)].
26. Siegman *et al.*, *IEEE J. Quantum Electron.* **27**, 1098 (1991).
27. Measurement of the x-ray beam profile at different positions or direct interferometric measurement of its spatial coherence will obviate the need for this assumption.
28. C. Kan and N. H. Burnett, unpublished results.
29. The electric field of a light pulse can be described in terms of a carrier of frequency ω_0 and a time-varying envelope of amplitude $A(t)$: $E(t) = A(t)\exp[-i(\omega_0 t + \psi)]$. This decomposition can be used to pulse durations down to the carrier oscillation cycle [T. Brabec and F. Krausz, *Phys. Rev. Lett.* **78**, 3282 (1997)]. The parameter ψ is the relative carrier phase. It determines the position of the carrier with respect to the envelope.
30. L. Xu *et al.*, *Opt. Lett.* **21**, 2008 (1996).

31. We are indebted to A. J. Schmidt for his encouragement and T. Brabec for useful discussions. K. Ferencz (Research Institute for Solid State Physics, Budapest, Hungary) is gratefully acknowledged for manufacturing the silver foils. This research was supported by the Austrian Science Foundation under grants P-11109 and Y44-PHY.

21 May 1997; accepted 9 September 1997

Superfluid Droplets on a Solid Surface

D. Ross, J. E. Rutledge, P. Taborek*

Photographs are presented of isolated superfluid helium-4 droplets prepared on a cesium surface, the only material known that is not wetted by superfluid helium. Although thermodynamic measurements show that the cesium surface is highly uniform, the contact angle of the droplets is extremely hysteretic and depends on whether the contact line is advancing or receding. Superfluid helium-4 droplets on an inclined surface do not flow downhill but rather are strongly pinned to the surface.

Superfluid He has unusual thermal and mechanical properties (*1*) and is well known for its ability to spread over surfaces and to flow without dissipation through even microscopic holes. Virtually all of the walls and surfaces used in earlier dissipationless flow experiments were observed to be wetted by superfluid He. This effect means that droplets on these substrates are unstable and immediately spread to form a smooth continuous film over the entire surface so that vapor and substrate are never in contact. Recent work (*2*) has shown that alkali metals are a special class of materials not completely wetted by superfluid He. In particular, Cs substrates can be used to prepare superfluid samples with a distinctly different topology consisting of a droplet with an edge where substrate, superfluid, and vapor meet at a three-phase contact line (*3*). We present here direct observations of isolated droplets of superfluid on a substrate (*4*). Both the static and the dynamic behaviors of the droplets were unusual. We found that the contact angle was an extremely hysteretic function of the volume of the drop. Perhaps most remarkable, superfluid droplets would not move across the surface until considerable force was applied to them. This result is surprising because solid surfaces are well known not to exert transverse forces on bulk superfluid or superfluid films without edges.

Our apparatus consisted of a substrate that can be rotated about a horizontal axis mounted in an optical cryostat with windows that provide an edge-on view of the substrate as well as a view from above at an angle of 60° from the normal. The substrate is a quartz microbalance with gold electrodes similar to those used in our earlier thermodynamic studies (*5*, *6*). Fifty atomic layers of Cs were vapor-deposited onto the quartz and gold surfaces of the microbalance at a rate of 0.01 layer per second. During the evaporation, the temperature of the substrate and the walls of the container were maintained below 6 K to maintain ultrahigh vacuum conditions. We used the microbalance to monitor the deposition and to perform thermodynamic characterizations of the surface; the wetting temperature was measured to be $T_w = 2.04$ K. A capillary tube (0.04 cm, outside diameter) attached to a source of room-temperature gas through a mass-flow controller provided a means of putting drops of superfluid on the surface. We maintained the system at liquid-vapor coexistence by filling the bottom of the container with bulk liquid ^{4}He. The drops were observed with a long-focal-distance microscope that provided a magnification of $\sim\times30$.

Figures 1 and 2 show a sequence of photos of superfluid drops on a Cs substrate at $T = 1.16$ K. Pictures taken with the microscope looking down on the substrate at an angle of 30° above the horizontal are shown in Fig. 1. The dark bar at the top of the pictures is the capillary tube, and the lower bar is its shadow. The tube was left in contact with the superfluid drop so that fluid could be added and withdrawn. This geometry is conventional for contact-angle measurements and typically yields the advancing and receding

Department of Physics and Astronomy, University of California, Irvine, CA 92697, USA.

*To whom correspondence should be addressed.